Correspondence to:

S. Sobhkhiz-Miandehi,
sahar@gfz-potsdam.de

Planetary Wave Signature in Low Latitude Sporadic E Layer Obtained From Multi-Mission Radio Occultation Observations

S. Sobhkhiz-Miandehi[1,2] [ID], Y. Yamazaki[3] [ID], C. Arras[1,4], Y. Miyoshi[5] [ID], H. Shinagawa[5,6] [ID], and A. P. Jadhav[7]

[1]GFZ German Research Centre for Geosciences, Potsdam, Germany, [2]University of Potsdam, Potsdam, Germany, [3]IAP Leibniz Institute of Atmospheric Physics, Kühlungsborn, Germany, [4]Berlin University of Technology, Berlin, Germany, [5]Kyushu University, Fukuoka, Japan, [6]National Institute of Information and Communications Technology, Tokyo, Japan, [7]Indian Institute of Geomagnetism, Navi Mumbai, Maharashtra, India

Abstract The Sporadic E layer or Es is an ionospheric phenomenon characterized by enhancements in electron density within 90–120 km above the Earth's surface. Based on the wind shear theory, the formation of Es layers is associated with vertical shears in the horizontal wind, in the presence of the Earth's magnetic field. This study explores the role of planetary waves on inducing these vertical shears and subsequently shaping Es layers. Our investigations benefit from a large amount of data facilitated by the FORMOSAT-7/COSMIC2 and Spire missions, which offer extensive global coverage. A wave analysis is applied to the Es intensity as represented by the S4 index derived from radio occultation measurements, in search of potential planetary wave signatures. Additionally, measurements from Aura/MLS are used to analyze corresponding spectra for the geopotential height, enabling a comparative examination of planetary wave signatures in the Es layer and geopotential height variations. The findings reveal westward and eastward wave components with specific wavenumbers and periods, suggesting the involvement of westward propagating quasi 6-day, quasi 4-day planetary waves, and eastward propagating Kelvin waves with a period of around 3 days in Es layer formation at low latitudes.

1. Introduction

Sporadic E (Es) layer is a phenomenon characterized by thin patches of enhanced electron density detected in the lower thermosphere, situated approximately 90–120 km above the Earth's surface (Haldoupis, 2011; Mathews, 1998; Whitehead, 1989; Wu et al., 2005). Es occurrences are commonly observed during daytime in local summer at mid- and low latitudes (Arras, 2010; Arras et al., 2010; Christakis et al., 2009; Haldoupis, 2012; Haldoupis et al., 2007). The significance of studying Es layers arises from their potential impact on the propagation of radio waves in communication and navigation systems, a topic explored since the mid-twentieth century (Macleod, 1966; Whitehead, 1961, 1970, 1989, 1989, 1989).

The formation of the Es layer is interpreted by the "wind shear" theory, initially proposed by Whitehead (1961) and Axford and Cunnold (1966). This theory suggests that vertical shears in the horizontal wind, combined with the Earth's magnetic field, result in the convergence of metallic ions (such as Fe+, Na+, and Ca+) in the ionospheric dynamo region, generating thin layers of enhanced ionization. The main source of metal species in the atmosphere is the ablation of meteoroids that globally occur between approximately 80 and 100 km (e.g., Vondark et al., 2008). Metallic ions are created through various chemical processes (e.g., Feng et al., 2013; Langowski et al., 2015).

Over the years, studies of Es have utilized various measurement techniques, including ionosonde recordings, incoherent and coherent scatter radars, and in situ measurements with rockets, all extensively discussed in review papers (Haldoupis, 2011; Mathews, 1998; Whitehead, 1989). With the advancement of GPS radio occultation technology in the past two decades, satellite observations have gained popularity in studies of Es layers for their capability to provide global data coverage (Arras et al., 2008; Igarashi et al., 2001; Wu et al., 2005). Recent studies employing global satellite observations, such as those by Yamazaki et al. (2022) and Sobhkhiz-Miandehi et al. (2022), have affirmed the wind shear theory as the primary mechanism for Es formation and its associated tidal variation.

At low and mid-latitudes, atmospheric tides, including solar and lunar tides with periods corresponding to a solar or lunar day and their harmonics, induce vertical shears of zonal wind. Several studies have explored the tidal structures in the Es layer. Studies from the 1970s revealed diurnal and semidiurnal tidal variations in Es occurrence rate (Harris & Taur, 1972; Mathews & Bekeny, 1979; Tarpley & Matsushita, 1971). Christakis et al. (2009) emphasized that the tidal signature in Es layer is observed at various altitudes depending on the local time and season. Observational studies have identified various migrating (sun-synchronous) tidal components, including diurnal, semidiurnal (Arras et al., 2009; Haldoupis et al., 2004; Oikonomou et al., 2014), terdiurnal, and quarterdiurnal (Fytterer et al., 2013, 2014; Jacobi et al., 2019), in the occurrence of the Es layer. Recent radio occultation observations have also demonstrated non-migrating tidal signature in Es occurrence rates (Sobhkhiz-Miandehi et al., 2022).

Numerous studies have utilized wind models, comparing them with radio occultation measurements of Es to demonstrate the correspondence of neutral wind shear with Es (e.g., Chu et al., 2014; Liu et al., 2018; Qiu et al., 2019, 2023; Yeh et al., 2014). Comparisons between Es observations and local wind measurements have confirmed the presence of tidal signature in Es layers (Arras et al., 2009; Fytterer et al., 2013; Jacobi & Arras, 2019; Yamazaki et al., 2022). Shinagawa et al. (2017) used GAIA (Ground-to-topside model of Atmosphere and Ionosphere for Aeronomy) model simulations to calculate the vertical ion convergence rate, revealing geographical and seasonal variations in vertical wind shears that are necessary for the Es formation. Andoh et al. (2020) simulated the day-to-day variability of Es at mid-latitudes, employing a numerical model of metallic ions driven by winds from the GAIA model. Additionally, some numerical studies focused on the role of atmospheric diurnal and semidiurnal tides for the Es formation (Andoh et al., 2023; Resende et al., 2017).

In addition to atmospheric tides, planetary waves significantly influence the vertical wind shear in the lower thermosphere (Haldoupis & Pancheva, 2002). Planetary waves represent global-scale oscillations in atmospheric parameters such as temperature, pressure, density, and neutral winds. They are commonly observed in the mesosphere and lower thermosphere (MLT) region with periods typically ranging from 2 to 20 days (Forbes, 1995; He et al., 2024; Salby, 1984). Commonly observed westward-propagating planetary waves with zonal wavenumber 1 have periods of approximately 5–7 days, 9–11 days, and 14–16 days, known as the quasi-6-day wave (Q6DW; Forbes & Zhang, 2017; Gan et al., 2018; Qin et al., 2021), quasi-10-day wave (Q10DW; Forbes & Zhang, 2015; Yamazaki & Matthias, 2019), and quasi-16-day wave (Q16DW; Fan et al., 2022; Day et al., 2011), respectively. Additionally, there are westward-propagating waves with a zonal wavenumber of 2 and a period of about 4 days, known as the quasi-4-day wave (Q4DW; Yamazaki et al., 2021; Ma et al., 2020). Equatorial Kelvin waves, on the other hand, are eastward-propagating global-scale waves that are trapped equatorially and excited by tropical convective processes (Forbes, 2000). Among Kelvin waves, ultra-fast Kelvin (UFKW) waves with a zonal wavenumber of 1 and a period of about 3 days are frequently detected in the MLT region (Davis et al., 2012; Forbes et al., 2009; Liu et al., 2019).

Linear wave theory (Chapman & Lindzen, 2012; Forbes, 1995; Longuet-Higgins, 1968) forms the foundation for understanding these atmospheric waves. The theory utilizes linearized equations to describe atmospheric wave motions, assuming a simplified atmosphere without dissipation and zonal mean winds. It is predicted that the Earth's atmosphere can support a series of normal-mode oscillations. Westward-propagating Q6DW, Q10DW, Q16DW and Q4DW in the MLT region are often regarded as manifestations of (1,1), (1,2), (1,3), and (2,2) normal modes, respectively, predicted by the linear wave theory. Observed wave characteristics, however, show some deviations from theoretical predictions, because of simplifications employed in the theory (Salby, 1981a, 1981b). For instance, the phase of theoretical normal modes does not vary with height, while observed Q6DW, Q10DW, Q16DW, and Q4DW have finite vertical wavelengths on the order of tens of kilometers in the MLT region. Since their phases are altitude dependent, they can contribute to the vertical shear of neutral winds, which would affect Es (Salby, 1981a).

Numerous studies have examined long-period oscillations in the ionospheric D (e.g., Cheng et al., 2021; Jacobi et al., 1998; Luo et al., 2000; Pancheva et al., 1991), E (e.g., Kishore et al., 2004; Shalimov & Haldoupis, 2002), and F regions (e.g., Altadill & Apostolov, 2003; Forbes et al., 2018; Laštovička, 1997; Laštovička et al., 2003; Yue et al., 2021), attributing them to planetary waves.

In the late 20th century, research findings indicate that planetary waves play a role in the formation of the Es layer (Tsunoda et al., 1998; Voiculescu et al., 1999). Tsunoda et al. (1998) and Voiculescu et al. (1999) were the first to provide evidence linking Es occurrences to planetary waves. They observed modulations in planetary waves

activity in the E region coherent backscatter, as detected by HF and VHF radars. Confirming the influence of planetary waves on Es, Voiculescu et al. (2000) extended their study using the data of a longer period. Shalimov et al. (1999) proposed a physical mechanism for Es formation driven by planetary waves, and later, Shalimov and Haldoupis (2002) introduced a theoretical model explaining how the large-scale accumulation of mid-latitude E region, driven by horizontal wind shear due to planetary waves, leads to Es layer formation. Haldoupis and Pancheva (2002) presented the first experimental evidence for the involvement of planetary waves in Es layer formation using foEs measurements from various ionosonde stations across different longitudinal sectors. Their results revealed a 7-day wave oscillation in Es layer occurrence. Moreover, Pancheva et al. (2003) demonstrated that Es layers are indirectly influenced by planetary waves through the nonlinear interaction of diurnal and semidiurnal tides with planetary waves. Haldoupis et al. (2004) expanded on this, developing a methodology to quantify the impact of tidal and planetary waves periodicities on sporadic E. Additionally, some ground-based studies employing wavelet analysis have shown quasi 6-day oscillations in Es occurrence (Pignalberi et al., 2015; Zuo & Wan, 2008; Zuo et al., 2009). Despite these studies indicating the impact of different types of planetary waves on the formation of the Es layer, our understanding remains incomplete. This is because previous research has mainly relied on ground-based observations, without considering the zonal structure (i.e., zonal wavenumber) and propagation direction (i.e., eastward or westward) of the wave. This paper addresses this gap by analyzing radio occultation measurements from two different satellite missions and identifying planetary wave signatures in Es based on the Fourier-wavelet analysis introduced by Yamazaki (2023). Unlike previous studies, this method can provide information not only on the period of oscillation but also on the zonal wavenumber and the direction of propagation (i.e., eastward or westward). We mainly focus on the low latitude region, where the radio occultation data are most abundant, and planetary wave signatures in Es are found to be prominent. Additionally, we analyze the geopotential height (GPH) measurements of the Microwave Limb Sounder on the Aura satellite (Aura/MLS), enabling a comparison between the planetary wave signatures in the Es layer and those in MLT dynamics represented by GPH.

2. Data and Method

For many years, studies on the Es layer primarily relied on ground-based observations such as ionosondes (Piggott, 1972; Wakai et al., 1987; Whitehead, 1989). Ionosondes remain in use due to their ability to provide high temporal resolution at specific locations. However, in the last two decades, GNSS radio occultation (RO) technique has emerged as a groundbreaking tool not only for Es layer studies but also for probing the atmosphere-ionosphere system (Arras et al., 2022; Jacobi et al., 2023; Qiu et al., 2019; Yu et al., 2022). Distinguishing itself from ground-based techniques, GNSS radio occultation offers global coverage and improved spatial resolution (Sobhkhiz-Miandehi et al., 2023). This technique relies on receiving GNSS signals transmitted through the Earth's atmosphere via a low Earth orbiting (LEO) satellite. Atmospheric refraction causes a bending in GNSS signals, and the measurement of this bending angle is crucial. It contains valuable information on various atmospheric parameters, including electron density, temperature, pressure, and water vapor profiles (Hajj et al., 2002).

An increasing number of satellites are now equipped with GNSS RO receivers. For this research, we utilized data from two satellite missions in the year 2022, including a total of 3,919,329 RO profiles. The first data set is derived from the FORMOSAT-7/COSMIC2 mission (Schreiner et al., 2020), involving six LEO satellites launched in June 2019. These satellites operate in inclined orbits of 24° at the altitude of 550 km and provide around 6000 RO profiles daily. Alongside tracking GPS signals, they also capture GLONASS signals. Additionally, our data set incorporates measurements obtained from satellites launched by the commercial company Spire in autumn 2021. The Spire constellation operates in inclination angles of 51.6°, 83°/85°, and 37° at the altitude of 500 km. Presently, it delivers around 4,000 RO profiles daily on a global scale. These satellites are designed to receive signals from various GNSS constellations, including GPS, Galileo, and GLONASS (Bowler, 2020; Masters et al., 2019).

The primary cause of scintillation in the signal-to-noise ratio (SNR) at E-region heights is generally attributed to the plasma density gradient resulting from the presence of Es. Previous studies have employed various methods to extract SNR and Es occurrence information from radio occultation profiles (Arras & Wickert, 2018; Chu et al., 2014; Gooch et al., 2020; Niu et al., 2019; Yu et al., 2022). Additionally, research has established a correlation between the S4 index, derived from radio occultation SNR data, and the Es layer observed by ionosondes (Arras & Wickert, 2018; Resende et al., 2018; Sobhkhiz-Miandehi et al., 2023; Wang et al., 2021). In this study,
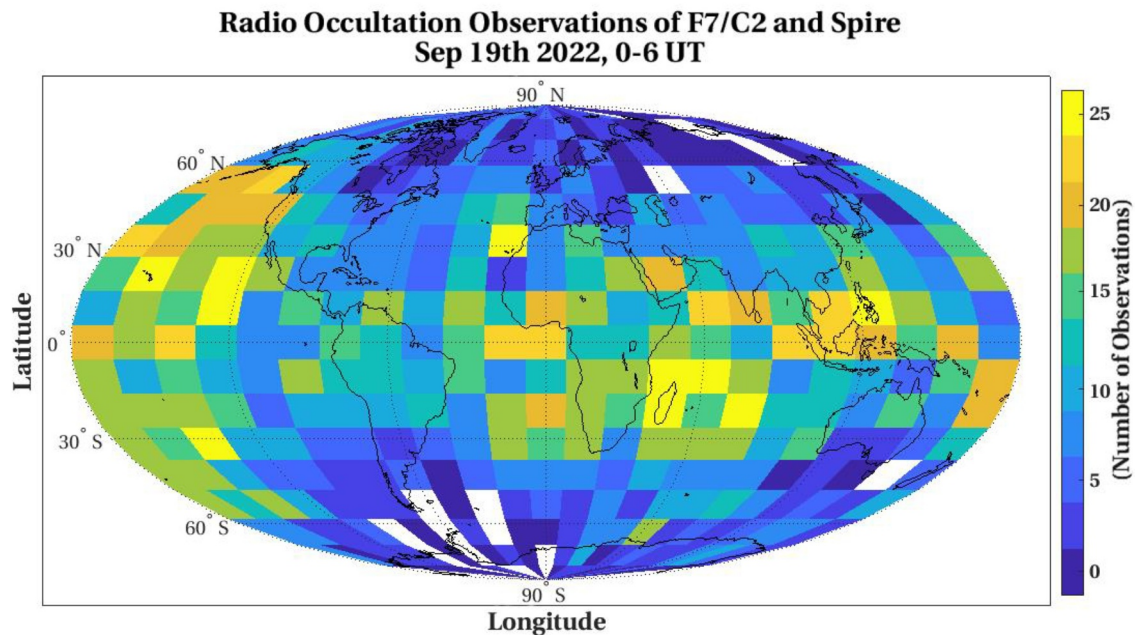
Figure 1. The total number of observations at each grid (10°Latitude × 15°Longitude) during one sample epoch of 6 hr.

we have used the S4 index of each RO profile, which is defined as the normalized ratio of the standard deviation of signal intensity fluctuations to the mean signal intensity.

We employed the Fourier-wavelet method described by Yamazaki (2023) to extract eastward- and westward-propagating wave components of the S4 index and GPH with various zonal wavenumbers. The Fourier-wavelet analysis involves a Fourier analysis in longitude and a wavelet analysis in time, providing amplitude spectra for eastward- and westward-propagating waves with different zonal wavenumbers. It requires uniformly gridded data as a function of time and longitude at a given latitude. To apply the Fourier-wavelet analysis, the data have been divided into grids of 10° latitude by 15° longitude, with a 6-hr time step. As illustrated in Figure 1, the number of observations is reduced at high latitudes due to the limited latitudinal coverage of FORMOSAT-7/COSMIC2, with the best coverage concentrated between 50° north and south. Therefore, our analysis is limited within this latitude range.

Aura is an ongoing NASA satellite mission in a sun-synchronous low Earth orbit, launched in July 2004. The Microwave Limb Sounder (MLS) onboard the Aura satellite (Schwartz et al., 2008; Waters et al., 2006) provides measurements of several atmospheric parameters, including GPH, temperature, and water vapor, across pressure levels ranging from 1,000 hPa (near Earth's surface) to 0.00001 hPa (~129 km). This study utilizes the Level 2 Version 4.2 GPH data at the pressure level of 0.001 hPa, corresponding to an altitude of approximately 95 km, to examine planetary wave activity in the MLT region. Previous studies have shown that Aura/MLS GPH data at this height can resolve various types of planetary waves (e.g., Qin et al., 2024; Yamazaki, 2018), which potentially affect higher altitudes, that is, the ionosphere. Our Aura/MLS data analysis procedure follows that in Jadhav et al. (2024).

3. Results

Applying Fourier-wavelet analysis on the average S4 values calculated over each 6-hr interval within each 10° latitude by 15° longitude grid, we obtained spectra of westward/eastward propagating wave components with a specific zonal wavenumber at different periods. The chosen altitude range for S4 analysis in this study is 105 ± 5 km, typically corresponding to the altitude of maximum Es occurrence and high-intensity Es (Haldoupis et al., 2006). At these altitudes, vertical shear of the zonal wind plays a leading role for the formation of Es, and vertical shear of the meridional wind plays only a secondary role.
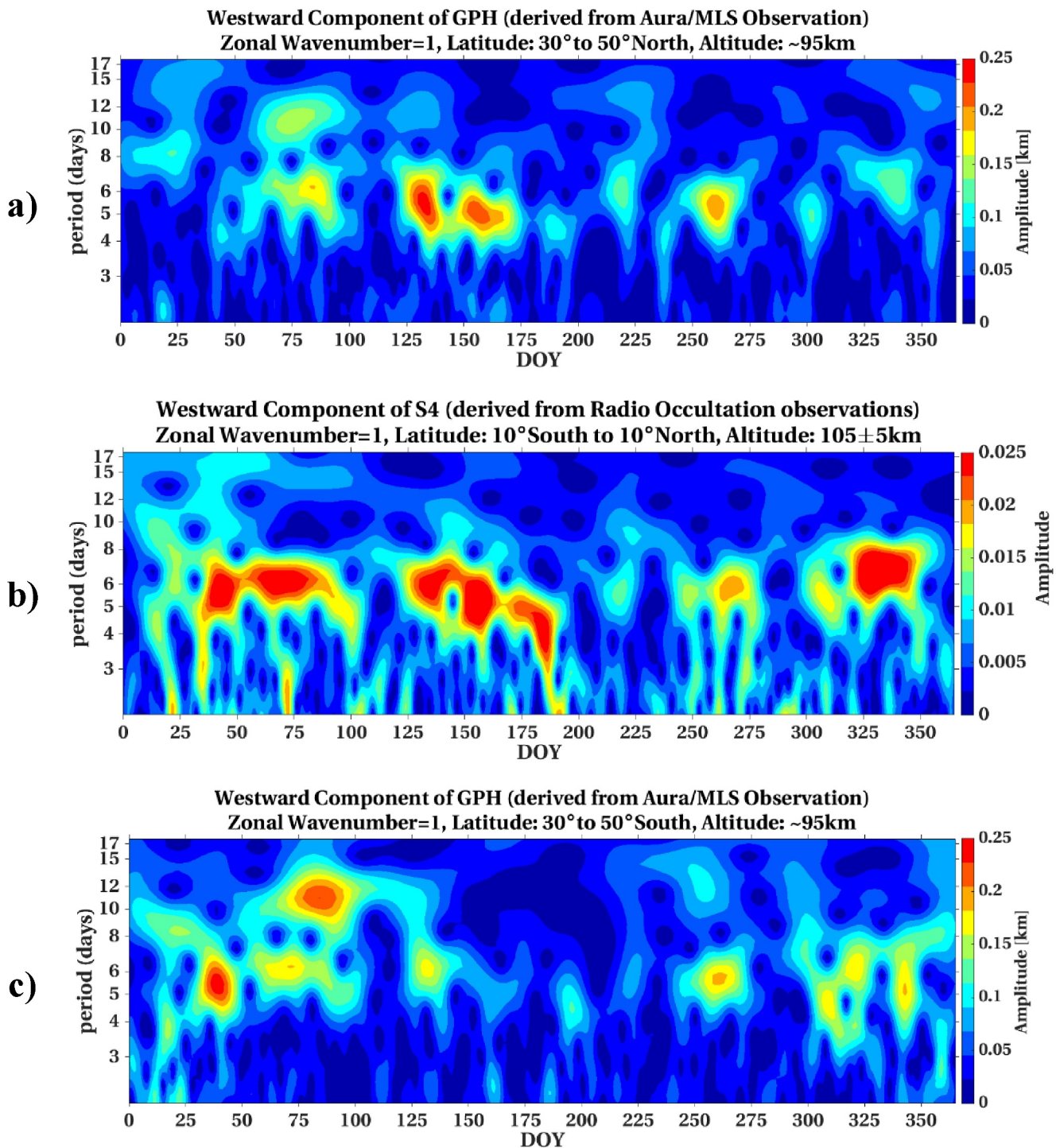
Figure 2. Temporal variations in the westward component of (a) GPH (derived from Aura/MLS observations) at the altitude of ~95 km and latitude of 30°–50° north, (b) S4 values (derived from radio occultation observations of F7/C2 and Spire) at the altitude of 105 ±5 km and latitude of 10° south–10° north, and (c) GPH (derived from Aura/MLS observations) at the altitude of ~95 km and latitude of 30°–50° south, with a zonal wavenumber of 1, during the year 2022.

Figure 2 compares Fourier-wavelet spectra obtained from GPH and S4 for the westward-propagating wave component with zonal wavenumber 1 (W1). Figures 2a and 2c show W1 amplitudes in GPH at northern and southern mid latitudes, respectively, at an altitude of ~95 km. W1 activity at a period of ~6 days is relatively strong, which can be attributed to the Q6DW. While the amplitude of the Q6DW in GPH is known to be largest at

mid latitudes, its amplitude in the zonal wind peaks at the equator (e.g., Miyoshi & Yamazaki, 2020). Thus, the influence of the Q6DW on Es might be observed at equatorial latitudes. Figure 2b presents the W1 amplitude in S4 over the equator. Enhanced W1 activity with a period of ∼6 days observed in S4 during February and December aligns with Q6DW events in GPH in the Southern Hemisphere. Similarly, W1 in S4 with a ∼6-day period during May and June is also evident in GPH in the Northern Hemisphere. The consistency between Q6DW activity in low-latitude S4 and mid-latitude GPH is notably observed in both hemispheres during March and September, which indicates the modulation of Es by Q6DW.

Figure 3 is the same as Figure 2 except for the westward-propagating component with zonal wavenumber 2 (W2). In the low latitude region, the S4 spectrum shown in Figure 3b reveals persistent W2 activity at periods of 3–6 days. Sometimes concurrent W2 activity is observed in GPH at mid latitudes (Figures 3a and 3c) at a period of ∼4 days, indicating the Q4DW and its influence on Es. The latitudinal structure of Q4DW is known to be similar to that of Q6DW (Yamazaki et al., 2021). That is, the amplitude in GPH is largest at mid latitudes, while the amplitude in the zonal wind peaks at the equator.

To examine Kelvin wave signatures in Es, we conducted a similar analysis to that presented in Figures 2 and 3 except for eastward propagating wave components around the equatorial region. Unlike the Q6DW and Q4DW, the amplitude of equatorial Kelvin waves is largest at the equator in both GPH and zonal wind (e.g., Forbes, 2000). Thus, we compare Fourier-wavelet spectra of GPH and S4 over the equator. In Figure 4a, temporal variations of the eastward propagating wave component with zonal wavenumber 1 (E1) in S4 reveal the highest amplitude for waves with periods around 3 days, indicating a potential sign of UFKW in Es. Additionally, the E1 amplitude in GPH at the equator also exhibits relatively high wave activity with a period of around 3 days, as shown in Figure 4b. This suggests that the presence of 3-day E1 waves in Es is a result of the UFKW from the MLT region, as observed in GPH data. The temporal variations of the eastward propagating wave component with zonal wavenumber 2 (E2) in S4 were also compared with those in GPH; however, these results are not shown here as they did not demonstrate high correlation.

The findings indicate a distinct quasi 6-day wave oscillation with zonal wavenumber 1 and a quasi 4-day wave oscillation with wave number 2 in equatorial S4 values and mid-latitude GPH variations. Additionally, a UFKW is evident in both parameters at the equator. To enhance our understanding of the latitudinal variations of these wave components in Es and GPH, we present in Figure 5 latitude versus period plots of Fourier-wavelet spectra averaged over the time period January–December 2022. The quasi 6-day and quasi 4-day wave oscillations, evident in S4 as shown in Figures 5a and 5c reach their maximum amplitude at low latitude regions. In contrast, the 6-day wave component in GPH, depicted in Figure 5b, increases around mid-latitude regions. In Figure 5d, 4-day wave component of GPH is not clear due to the transient nature of this wave. Since Figure 5d shows an annual average, it makes the 4-day wave difficult to distinguish. Furthermore, Figures 5e and 5f highlight the presence of Ultra-Fast Kelvin Waves (UFKW) in both the GPH and S4 values, particularly around the equatorial region.

4. Discussion

The results reveal the presence of global-scale wave components in both S4 and GPH. Overall, the consistency between the wave components in S4 and those in GPH suggests the involvement of Q6DW, Q4DW, and UFKW in the formation of the Es layer.

Observations indicate that both Q6DW and Q4DW typically exhibit a vertical wavelength of 60–70 km (Forbes & Zhang, 2017; Gu et al., 2014; Yamazaki et al., 2021). This is comparable with the vertical wavelengths of various diurnal and semidiurnal tides (approximately 40–90 km) that propagate from the lower atmosphere to the ionospheric dynamo region (Oberheide et al., 2011). These tides are known to play a significant role in modulating the vertical convergence of metallic ions, thus influencing Es layers at low and middle latitudes (Sobhkhiz-Miandehi et al., 2022). Thus, it can be expected that the vertical wind shears associated with Q6DW and Q4DW also play a role in modulating Es layers.

Equatorial Kelvin waves are typically generated by latent heating from tropical convection. They are eastward-propagating, with their strongest zonal wind amplitudes observed around the equator (Forbes, 2000). Kelvin waves in the lower thermosphere typically have a period of 2 and 3 days (e.g., Forbes et al., 2009; Lieberman &
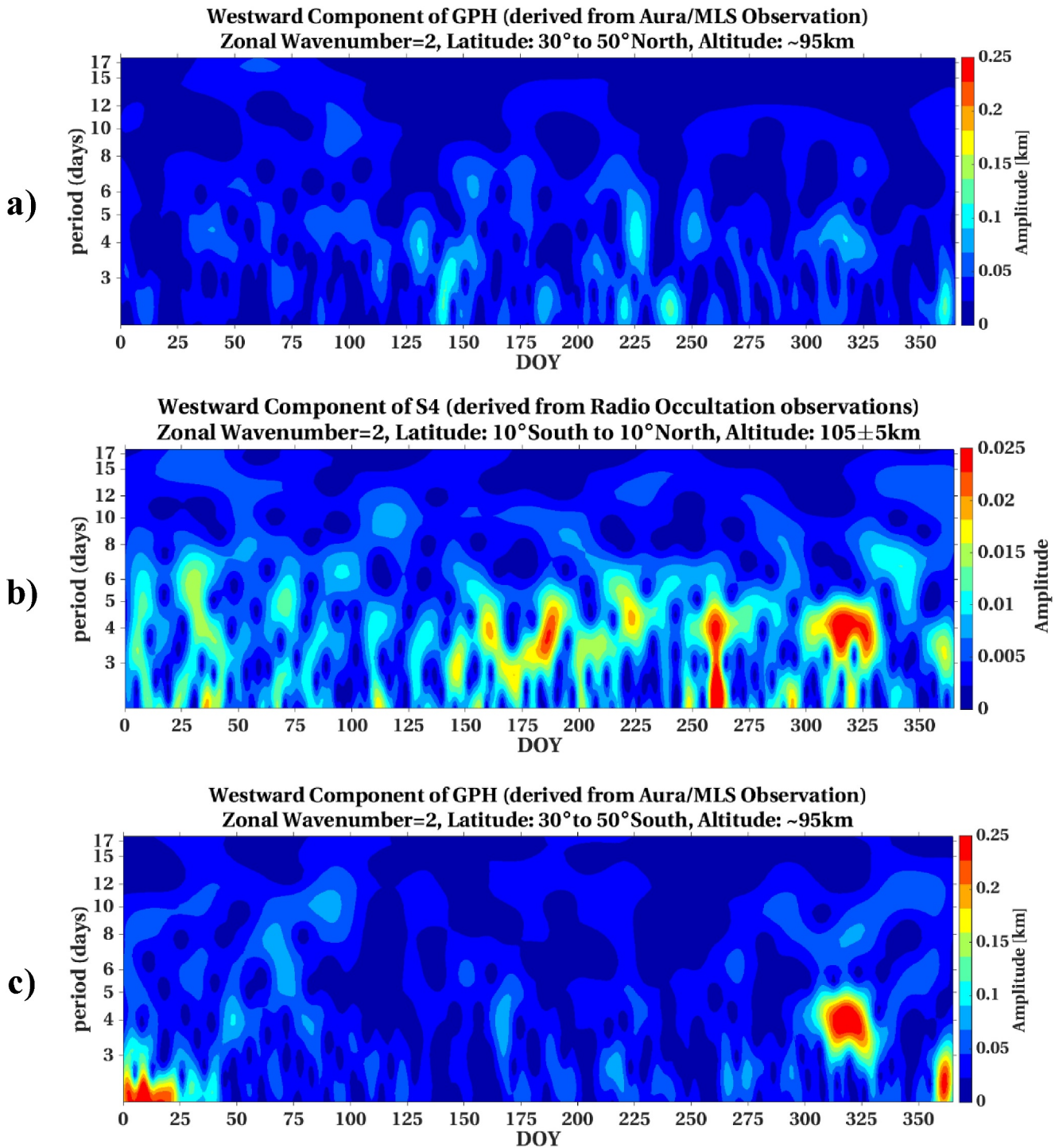
Figure 3. Temporal variations in the westward component of (a) GPH (derived from Aura/MLS observations) at the altitude of ~95 km and latitude of 30°–50° north, (b) S4 values (derived from radio occultation observations of F7/C2 and Spire) at the altitude of 105 ±5 km and latitude of 10° south–10° north, and (c) GPH (derived from Aura/MLS observations) at the altitude of ~95 km and latitude of 30°–50° south, with a zonal wavenumber of 2, during the year 2022.

Riggin, 1997) as longer period waves are prone to dissipation before reaching the thermosphere. The vertical wavelength of Kelvin waves with zonal wavenumber 1 and a period of 2 and 3 days is typically ranges from 35 to 45 km (Davis et al., 2012; Yamazaki et al., 2020), comparable to that of migrating diurnal tides. Therefore, it's possible that the vertical wind shears associated with UFKWs can effectively influence Es layers.
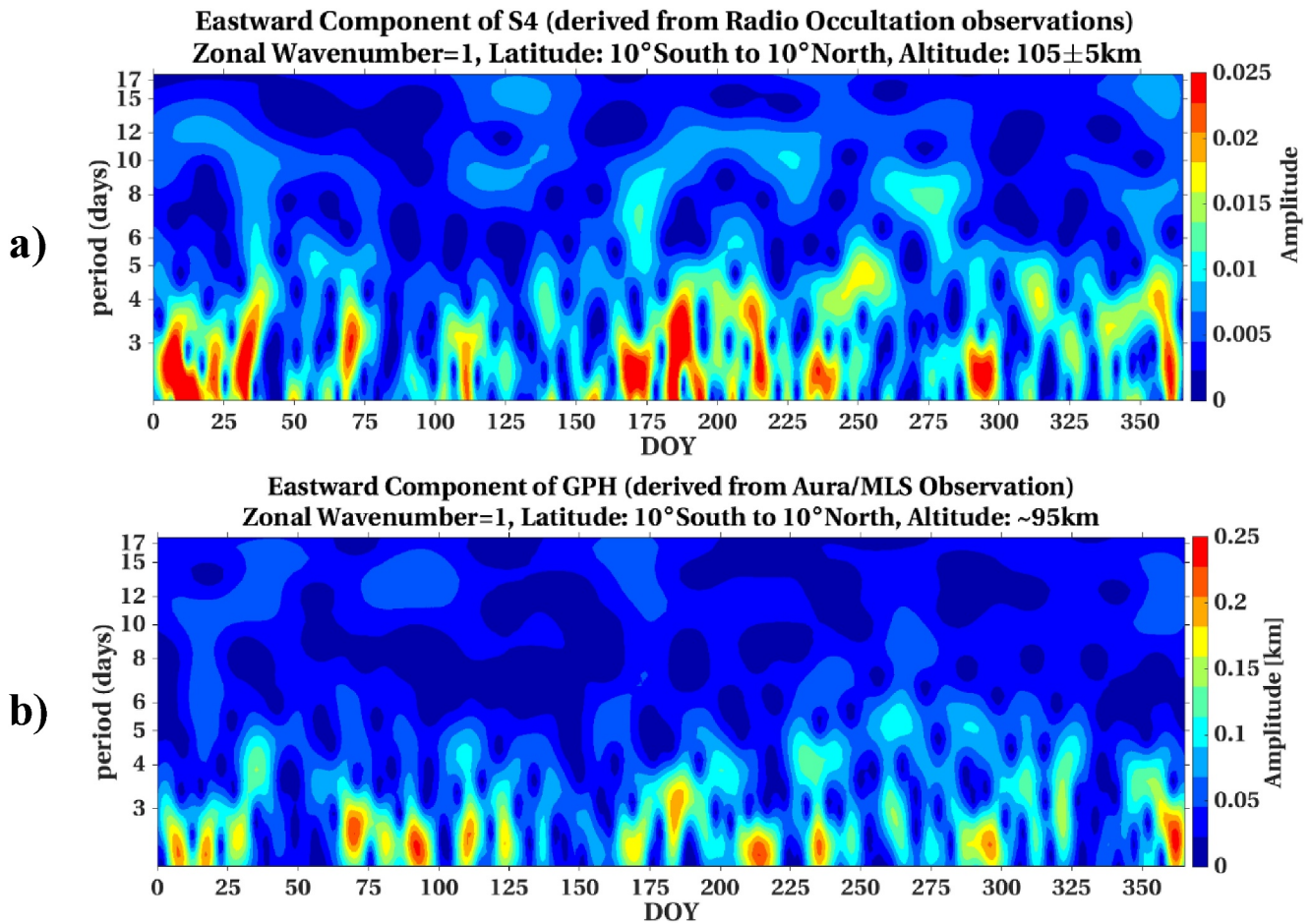
Figure 4. Temporal variations in the eastward component of (a) GPH (derived from Aura/MLS observations) at the altitude of ~95 km, and (b) S4 values (derived from radio occultation observations of F7/C2 and Spire) at the altitude of 105 ±5 km and latitude of 10° south–10° north with a zonal wavenumber of 1, during the year 2022.

According to the wind shear theory, the vertical convergence of metallic ions due to the vertical shear of the zonal wind is most effective when the magnetic inclination angle is small. However, the exception lies at the magnetic equator, where inclination angle is zero but Es layers cannot form due to the presence of the vertical electric field (Arras et al., 2022). Given that Q6DW, Q4DW, and UFKW exhibit maximum zonal wind perturbations at the equator, where the magnetic inclination angle is small, it's likely that their influence on Es layers is particularly efficient.

5. Conclusions

In this study, we explored the influence of planetary waves on Es layer using RO data from the FORMOSAT-7/COSMIC2 and Spire missions, comparing them with GPH data from the Aura/MLS satellite. Our investigation involved Fourier-wavelet analysis applied to S4 and GPH to assess the presence of different global-scale wave components. Here are the main findings:

1. We observed westward propagating wave components with zonal wavenumber 1 and a period of ~6 days and those with zonal wavenumber 2 and a period of ~4 days, in both S4 and GPH. This robust presence confirms the role of quasi 6-day and quasi 4-day planetary waves in the formation of the Es layer.
2. Eastward propagating wave components of zonal wavenumber 1, with a period around 3 days, were identified in both S4 and GPH. This consistent presence supports the involvement of UFKW in Es layer formation.
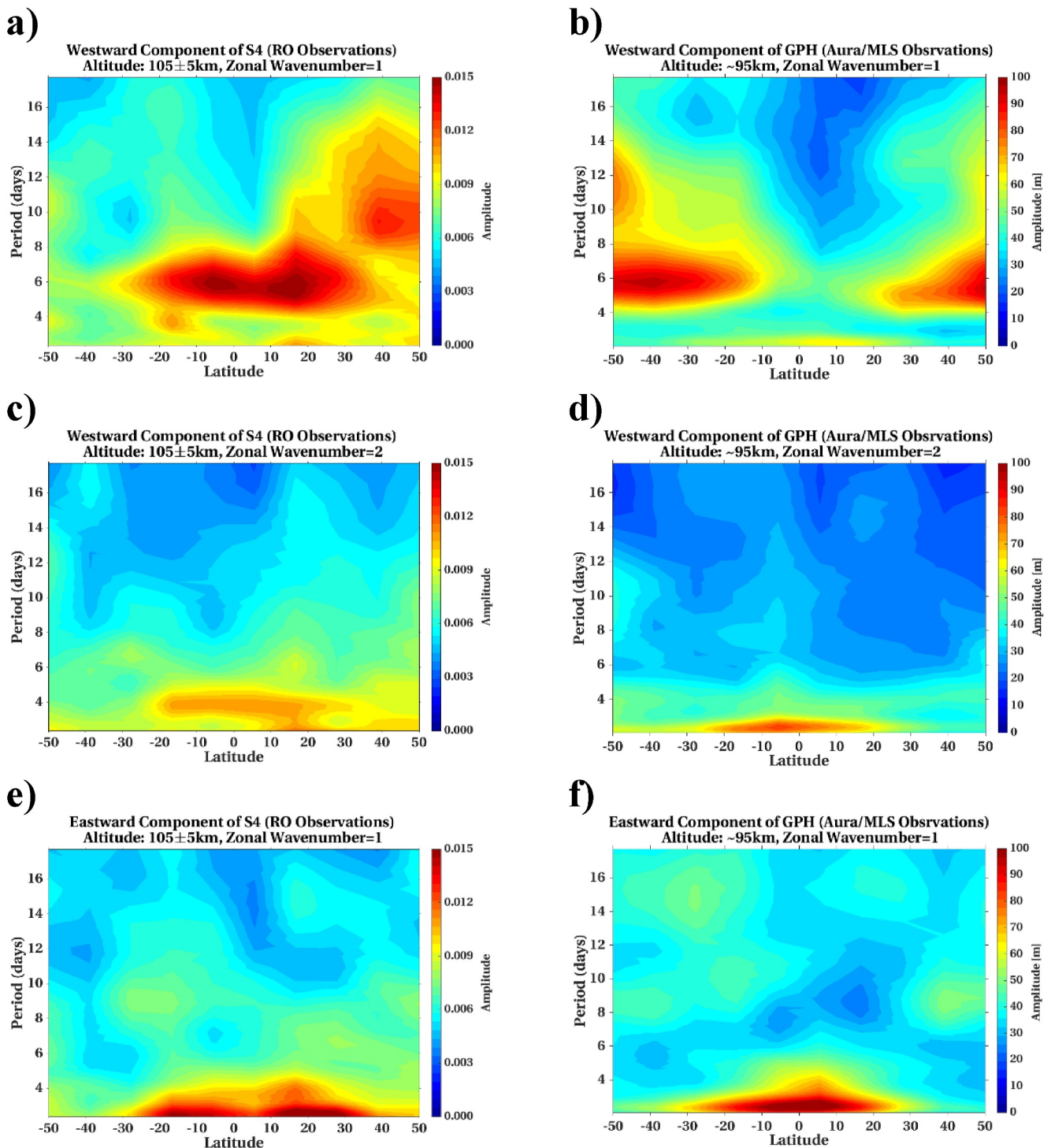
Figure 5. Latitudinal variations in the westward wave component with zonal wavenumber = 1 of (a) S4 at 105 ±5 km, (b) GPH at ~95 km, westward wave component with zonal wavenumber = 2 of (c) S4 at 105 ±5 km, (d) GPH at ~95 km, eastward wave component with zonal wavenumber = 1 of (e) S4 at 105 ±5 km, (f) GPH at ~95 km averaged over the whole year 2022.

Data Availability Statement

MATLAB and Python software for the Fourier-wavelet analysis are available in Yamazaki (2023b). Radio occultation data used in this study are the conPhs data product that can be accessed via UCAR website for both

Spire (Spire Repository, 2024) and F7/C2 (F7/C2 Spire Repository, 2024). Aura MLS GPH data has been made available by Goddard Earth Sciences Data and Information Services Center (Schwartz et al., 2008) and can be accessed in their website (GES DISC, 2024).

References

Altadill, D., & Apostolov, E. M. (2003). Time and scale size of planetary wave signatures in the ionospheric F region: Role of the geomagnetic activity and mesosphere/lower thermosphere winds. *Journal of Geophysical Research*, *108*(A11), 1403. https://doi.org/10.1029/2003ja010015

Andoh, S., Saito, A., & Shinagawa, H. (2023). Simulation of horizontal sporadic E layer movement driven by atmospheric tides. *Earth Planets and Space*, *75*(1), 86. https://doi.org/10.1186/s40623-023-01837-0

Andoh, S., Saito, A., Shinagawa, H., & Ejiri, M. K. (2020). First simulations of day-to-day variability of mid-latitude sporadic E layer structures. *Earth Planets and Space*, *72*(1), 1–9. https://doi.org/10.1186/s40623-020-01299-8

Arras, C. (2010). A global survey of sporadic E layers based on GPS Radio occultations by CHAMP, GRACE and FORMOSAT–3/COSMIC Deutsches GeoForschungsZentrum GFZ Potsdam].

Arras, C., Jacobi, C., & Wickert, J. (2009). Semidiurnal tidal signature in sporadic E occurrence rates derived from GPS radio occultation measurements at higher midlatitudes. *Annales Geophysicae*, *27*(6), 2555–2563. https://doi.org/10.5194/angeo-27-2555-2009

Arras, C., Jacobi, C., Wickert, J., Heise, S., & Schmidt, T. (2010). Sporadic E signatures revealed from multi-satellite radio occultation measurements. *Advances in Radio Science*, *8*(GHJ. 1-1/1-), 225–230. https://doi.org/10.5194/ars-8-225-2010

Arras, C., Resende, L. C. A., Kepkar, A., Senevirathna, G., & Wickert, J. (2022). Sporadic E layer characteristics at equatorial latitudes as observed by GNSS radio occultation measurements. *Earth Planets and Space*, *74*(1), 163. https://doi.org/10.1186/s40623-022-01718-y

Arras, C., & Wickert, J. (2018). Estimation of ionospheric sporadic E intensities from GPS radio occultation measurements. *Journal of Atmospheric and Solar-Terrestrial Physics*, *171*, 60–63. https://doi.org/10.1016/j.jastp.2017.08.006

Arras, C., Wickert, J., Beyerle, G., Heise, S., Schmidt, T., & Jacobi, C. (2008). A global climatology of ionospheric irregularities derived from GPS radio occultation. *Geophysical Research Letters*, *35*(14), L14809. https://doi.org/10.1029/2008gl034158

Axford, W., & Cunnold, D. (1966). The wind-shear theory of temperate zone sporadic E. *Radio Science*, *1*(2), 191–197. https://doi.org/10.1002/rds196612191

Bowler, N. E. (2020). An assessment of GNSS radio occultation data produced by Spire. *Quarterly Journal of the Royal Meteorological Society*, *146*(733), 3772–3788. https://doi.org/10.1002/qj.3872

Chapman, S., & Lindzen, R. S. (2012). *Atmospheric tides: Thermal and gravitational*. Springer Science & Business Media.

Cheng, H., Huang, K., Liu, A. Z., Zhang, S., Huang, C., & Gong, Y. (2021). A quasi-27-day oscillation activity from the troposphere to the mesosphere and lower thermosphere at low latitudes. *Earth Planets and Space*, *73*(1), 1–13. https://doi.org/10.1186/s40623-021-01521-1

Christakis, N., Haldoupis, C., Zhou, Q., & Meek, C. (2009). Seasonal variability and descent of mid-latitude sporadic E layers at Arecibo. *Annales Geophysicae*, *27*(3), 923–931. https://doi.org/10.5194/angeo-27-923-2009

Chu, Y.-H., Wang, C., Wu, K., Chen, K., Tzeng, K., Su, C.-L., et al. (2014). Morphology of sporadic E layer retrieved from COSMIC GPS radio occultation measurements: Wind shear theory examination. *Journal of Geophysical Research: Space Physics*, *119*(3), 2117–2136. https://doi.org/10.1002/2013ja019437

Davis, R. N., Chen, Y. W., Miyahara, S., & Mitchell, N. J. (2012). The climatology, propagation and excitation of ultra-fast Kelvin waves as observed by meteor radar, Aura MLS, TRMM and in the Kyushu-GCM. *Atmospheric Chemistry and Physics*, *12*(4), 1865–1879. https://doi.org/10.5194/acp-12-1865-2012

Day, K. A., Hibbins, R. E., & Mitchell, N. J. (2011). Aura MLS observations of the westward-propagating $s = 1$, 16-day planetary wave in the stratosphere, mesosphere and lower thermosphere. *Atmospheric Chemistry and Physics*, *11*(9), 4149–4161. https://doi.org/10.5194/acp-11-4149-2011

Fan, Y., Huang, C. M., Zhang, S. D., Huang, K. M., & Gong, Y. (2022). Long-term study of quasi-16-day waves based on ERA5 reanalysis data and EOS MLS observations from 2005 to 2020. *Journal of Geophysical Research: Space Physics*, *127*(4), e2021JA030030. https://doi.org/10.1029/2021ja030030

Feng, W., Marsh, D. R., Chipperfield, M. P., Janches, D., Höffner, J., Yi, F., & Plane, J. M. (2013). A global atmospheric model of meteoric iron. *Journal of Geophysical Research: Atmospheres*, *118*(16), 9456–9474. https://doi.org/10.1002/jgrd.50708

Forbes, J. M. (1995). Tidal and planetary waves. The upper mesosphere and lower thermosphere: A review of experiment and theory. *Geophysical Monograph Series*, *87*, 67–87.

Forbes, J. M. (2000). Wave coupling between the lower and upper atmosphere: Case study of an ultra-fast Kelvin Wave. *Journal of Atmospheric and Solar-Terrestrial Physics*, *62*(17–18), 1603–1621. https://doi.org/10.1016/s1364-6826(00)00115-2

Forbes, J. M., Maute, A., Zhang, X., & Hagan, M. E. (2018). Oscillation of the ionosphere at planetary-wave periods. *Journal of Geophysical Research: Space Physics*, *123*(9), 7634–7649. https://doi.org/10.1029/2018ja025720

Forbes, J. M., & Zhang, X. (2015). Quasi-10-day wave in the atmosphere. *Journal of Geophysical Research: Atmospheres*, *120*(21), 11079–11089. https://doi.org/10.1002/2015jd023327

Forbes, J. M., & Zhang, X. (2017). The quasi-6 day wave and its interactions with solar tides. *Journal of Geophysical Research: Space Physics*, *122*(4), 4764–4776. https://doi.org/10.1002/2017ja023954

Forbes, J. M., Zhang, X., Palo, S. E., Russell, J., Mertens, C. J., & Mlynczak, M. (2009). Kelvin waves in stratosphere, mesosphere and lower thermosphere temperatures as observed by TIMED/SABER during 2002–2006. *Earth Planets and Space*, *61*(4), 447–453. https://doi.org/10.1186/bf03353161

Fytterer, T., Arras, C., Hoffmann, P., & Jacobi, C. (2014). Global distribution of the migrating terdiurnal tide seen in sporadic E occurrence frequencies obtained from GPS radio occultations. *Earth Planets and Space*, *66*(1), 1–9. https://doi.org/10.1186/1880-5981-66-79

Fytterer, T., Arras, C., & Jacobi, C. (2013). Terdiurnal signatures in sporadic E layers at midlatitudes. *Advances in Radio Science*, *11*(YSA), 333–339. https://doi.org/10.5194/ars-11-333-2013

F7/C2 Repository. (2024). UCAR website [Dataset]. Retrieved from https://data.cosmic.ucar.edu/gnss-ro/cosmic2/nrt/level1b/

Gan, Q., Oberheide, J., & Pedatella, N. M. (2018). Sources, sinks, and propagation characteristics of the quasi 6-day wave and its impact on the residual mean circulation. *Journal of Geophysical Research: Atmospheres*, *123*(17), 9152–9170. https://doi.org/10.1029/2018jd028553

GES DISC. (2024). Goddard Earth sciences data and information services center website. Retrieved from https://disc.gsfc.nasa.gov/

Gooch, J. Y., Colman, J. J., Nava, O. A., & Emmons, D. J. (2020). Global ionosonde and GPS radio occultation sporadic-E intensity and height comparison. *Journal of Atmospheric and Solar-Terrestrial Physics*, *199*, 105200. https://doi.org/10.1016/j.jastp.2020.105200

Gu, S. Y., Liu, H. L., Li, T., Dou, X., Wu, Q., & Russell, J. M., III. (2014). Observation of the neutral-ion coupling through 6 day planetary wave. *Journal of Geophysical Research: Space Physics*, *119*(12), 10–376. https://doi.org/10.1002/2014ja020530

Hajj, G. A., Kursinski, E., Romans, L., Bertiger, W., & Leroy, S. (2002). A technical description of atmospheric sounding by GPS occultation. *Journal of Atmospheric and Solar-Terrestrial Physics*, *64*(4), 451–469. https://doi.org/10.1016/s1364-6826(01)00114-6

Haldoupis, C. (2011). A tutorial review on sporadic E layers. In *Aeronomy of the Earth's atmosphere and ionosphere* (pp. 381–394). Springer.

Haldoupis, C. (2012). Midlatitude sporadic E. A typical paradigm of atmosphere-ionosphere coupling. *Space Science Reviews*, *168*, 441–461. https://doi.org/10.1007/978-1-4614-5677-3_15

Haldoupis, C., Meek, C., Christakis, N., Pancheva, D., & Bourdillon, A. (2006). Ionogram height–time–intensity observations of descending sporadic E layers at mid-latitude. *Journal of Atmospheric and Solar-Terrestrial Physics*, *68*(3–5), 539–557. https://doi.org/10.1016/j.jastp.2005.03.020

Haldoupis, C., & Pancheva, D. (2002). Planetary waves and midlatitude sporadic E layers: Strong experimental evidence for a close relationship. *Journal of Geophysical Research*, *107*(A6), SIA3-1–SIA3-6. https://doi.org/10.1029/2001ja000212

Haldoupis, C., Pancheva, D., & Mitchell, N. J. (2004). A study of tidal and planetary wave periodicities present in midlatitude sporadic E layers. *Journal of Geophysical Research*, *109*(A2), A02302. https://doi.org/10.1029/2003ja010253

Haldoupis, C., Pancheva, D., Singer, W., Meek, C., & MacDougall, J. (2007). An explanation for the seasonal dependence of midlatitude sporadic E layers. *Journal of Geophysical Research*, *112*(A6), A06315. https://doi.org/10.1029/2007ja012322

Harris, R., & Taur, R. (1972). Influence of the tidal wind system on the frequency of sporadic-E occurrence. *Radio Science*, *7*(3), 405–410. https://doi.org/10.1029/rs007i003p00405

He, M., Forbes, J. M., Stober, G., Jacobi, C., Li, G., Liu, L., & Xu, J. (2024). Nonlinear interactions of planetary-scale waves in mesospheric winds observed at 52N latitude and two longitudes (arXiv:2406.05848). *arXiv*. https://doi.org/10.48550/arXiv.2406.05848

Igarashi, K., Nakamura, M., Wilkinson, P., Wu, J., Pavelyev, A., & Wickert, J. (2001). Global sounding of sporadic E layers by the GPS/MET radio occultation experiment. *Journal of Atmospheric and Solar-Terrestrial Physics*, *63*(18), 1973–1980. https://doi.org/10.1016/s1364-6826(01)00063-3

Jacobi, C., & Arras, C. (2019). Tidal wind shear observed by meteor radar and comparison with sporadic E occurrence rates based on GPS radio occultation observations. *Advances in Radio Science*, *17*, 213–224. https://doi.org/10.5194/ars-17-213-2019

Jacobi, C., Arras, C., Geißler, C., & Lilienthal, F. (2019). Quarterdiurnal signature in sporadic E occurrence rates and comparison with neutral wind shear. *Annales Geophysicae*, *37*(3), 273–288. https://doi.org/10.5194/angeo-37-273-2019

Jacobi, C., Kandieva, K., & Arras, C. (2023). Migrating and nonmigrating tidal signatures in sporadic E layer occurrence rates. *Advances in Radio Science*, *20*, 85–92. https://doi.org/10.5194/ars-20-85-2023

Jacobi, C., Schminder, R., & Kürschner, D. (1998). Planetary wave activity obtained from long-period (2–18 days) variations of mesopause region winds over Central Europe (52°N, 15°E). *Journal of Atmospheric and Solar-Terrestrial Physics*, *60*(1), 81–93. https://doi.org/10.1016/s1364-6826(97)00117-x

Jadhav, A. P., Yamazaki, Y., Gurubaran, S., Stolle, C., Conte, J. F., Batista, P. P., & Buriti, R. A. (2024). Quasi 16-day wave signatures in the interhemispheric field aligned currents: A new perspective toward atmosphere-ionosphere coupling. *Journal of Geophysical Research: Space Physics*, *129*(6), e2023JA032383. https://doi.org/10.1029/2023ja032383

Kishore, P., Namboothiri, S. P., Igarashi, K., Gurubaran, S., Sridharan, S., Rajaram, R., & Ratnam, M. V. (2004). MF radar observations of 6.5-day wave in the equatorial mesosphere and lower thermosphere. *Journal of Atmospheric and Solar-Terrestrial Physics*, *66*(6–9), 507–515. https://doi.org/10.1016/j.jastp.2004.01.026

Langowski, M. P., Von Savigny, C., Burrows, J. P., Feng, W., Plane, J. M. C., Marsh, D. R., et al. (2015). Global investigation of the Mg atom and ion layers using SCIAMACHY/Envisat observations between 70 and 150 km altitude and WACCM-Mg model results. *Atmospheric Chemistry and Physics*, *15*(1), 273–295. https://doi.org/10.5194/acp-15-273-2015

Laštovička, J. (1997). Observations of tides and planetary waves in the atmosphere-ionosphere system. *Advances in Space Research*, *20*(6), 1209–1222. https://doi.org/10.1016/s0273-1177(97)00774-6

Laštovička, J., Križan, P., Šauli, P., & Novotna, D. (2003). Persistence of the planetary wave type oscillations in foF2 over Europe. *Annales Geophysicae*, *21*(7), 1543–1552. https://doi.org/10.5194/angeo-21-1543-2003

Lieberman, R. S., & Riggin, D. (1997). High resolution Doppler imager observations of Kelvin waves in the equatorial mesosphere and lower thermosphere. *Journal of Geophysical Research*, *102*(D22), 26117–26130. https://doi.org/10.1029/96jd02902

Liu, G., England, S. L., & Janches, D. (2019). Quasi two-, three-, and six-day planetary-scale wave oscillations in the upper atmosphere observed by TIMED/SABER over ∼17 years during 2002–2018. *Journal of Geophysical Research: Space Physics*, *124*(11), 9462–9474. https://doi.org/10.1029/2019ja026918

Liu, Y., Zhou, C., Tang, Q., Li, Z., Song, Y., Qing, H., et al. (2018). The seasonal distribution of sporadic E layers observed from radio occultation measurements and its relation with wind shear measured by TIMED/TIDI. *Advances in Space Research*, *62*(2), 426–439. https://doi.org/10.1016/j.asr.2018.04.026

Longuet-Higgins, M. S. (1968). The eigenfunctions of Laplace's tidal equation over a sphere. *Philosophical Transactions of the Royal Society of London - Series A: Mathematical and Physical Sciences*, *262*(1132), 511–607. https://doi.org/10.1098/rsta.1968.0003

Luo, Y., Manson, A. H., Meek, C. E., Meyer, C. K., & Forbes, J. M. (2000). The quasi 16-day oscillations in the mesosphere and lower thermosphere at Saskatoon (52°N, 107°W), 1980–1996. *Journal of Geophysical Research*, *105*(D2), 2125–2138. https://doi.org/10.1029/1999jd900979

Ma, Z., Gong, Y., Zhang, S., Zhou, Q., Huang, C., Huang, K., et al. (2020). Study of a quasi 4-day oscillation during the 2018/2019 SSW over Mohe, China. *Journal of Geophysical Research: Space Physics*, *125*(7), e2019JA027687. https://doi.org/10.1029/2019ja027687

Macleod, M. A. (1966). Sporadic E theory. I. Collision-geomagnetic equilibrium. *Journal of the Atmospheric Sciences*, *23*(1), 96–109. https://doi.org/10.1175/1520-0469(1966)023<0096:seticg>2.0.co;2

Masters, D., Irisov, V., Nguyen, V., Duly, T., Nogués-Correig, O., Tan, L., et al. (2019). Status and plans for Spire's growing commercial constellation of GNSS science CubeSats. In *Proceedings of the Joint 6th ROM SAF User Workshop and 7th IROWG Workshop, Helsingør, Denmark*.

Mathews, J. (1998). Sporadic E: Current views and recent progress. *Journal of Atmospheric and Solar-Terrestrial Physics*, *60*(4), 413–435. https://doi.org/10.1016/s1364-6826(97)00043-6

Mathews, J. D., & Bekeny, F. (1979). Upper atmosphere tides and the vertical motion of ionospheric sporadic layers at Arecibo. *Journal of Geophysical Research*, *84*(A6), 2743–2750. https://doi.org/10.1029/ja084ia06p02743

Miyoshi, Y., & Yamazaki, Y. (2020). Excitation mechanism of ionospheric 6-day oscillation during the 2019 September sudden stratospheric warming event. *Journal of Geophysical Research: Space Physics*, *125*(9), e2020JA028283. https://doi.org/10.1029/2020ja028283

Niu, J., Weng, L. B., Meng, X., & Fang, H. X. (2019). Morphology of ionospheric sporadic E layer intensity based on COSMIC occultation data in the midlatitude and low-latitude regions. *Journal of Geophysical Research: Space Physics*, *124*(6), 4796–4808. https://doi.org/10.1029/2019ja026828

Oberheide, J., Forbes, J. M., Zhang, X., & Bruinsma, S. (2011). Climatology of upward propagating diurnal and semidiurnal tides in the thermosphere. *Journal of Geophysical Research*, *116*(A11), A11306. https://doi.org/10.1029/2011ja016784

Oikonomou, C., Haralambous, H., Haldoupis, C., & Meek, C. (2014). Sporadic E tidal variabilities and characteristics observed with the Cyprus Digisonde. *Journal of Atmospheric and Solar-Terrestrial Physics*, *119*, 173–183. https://doi.org/10.1016/j.jastp.2014.07.014

Pancheva, D., Haldoupis, C., Meek, C., Manson, A., & Mitchell, N. (2003). Evidence of a role for modulated atmospheric tides in the dependence of sporadic E layers on planetary waves. *Journal of Geophysical Research*, *108*(A5), 1176. https://doi.org/10.1029/2002ja009788

Pancheva, D., Schminder, R., & Laštovička, J. (1991). 27-day fluctuations in the ionospheric D-region. *Journal of Atmospheric and Terrestrial Physics*, *53*(11–12), 1145–1150. https://doi.org/10.1016/0021-9169(91)90064-e

Piggott, W. (1972). *Handbook of ionogram interpretation and reduction*. US Department of Commerce.

Pignalberi, A., Pezzopane, M., & Zuccheretti, E. (2015). A spectral study of the mid-latitude sporadic E layer characteristic oscillations comparable to those of the tidal and the planetary waves. *Journal of Atmospheric and Solar-Terrestrial Physics*, *122*, 34–44. https://doi.org/10.1016/j.jastp.2014.10.017

Qin, Y., Gu, S. Y., Dou, X., & Wei, Y. (2024). Unexpected global structure of quasi-4-day wave with westward zonal wavenumber 2 during the February 2023 unusual major sudden stratospheric warming with elevated stratopause. *Geophysical Research Letters*, *51*(13), e2024GL109682. https://doi.org/10.1029/2024gl109682

Qin, Y., Gu, S. Y., Teng, C. K. M., Dou, X. K., Yu, Y., & Li, N. (2021). Comprehensive study of the climatology of the quasi-6-day wave in the MLT region based on Aura/MLS observations and SD-WACCM-X simulations. *Journal of Geophysical Research: Space Physics*, *126*(1), e2020JA028454. https://doi.org/10.1029/2020ja028454

Qiu, L., Yamazaki, Y., Yu, T., Miyoshi, Y., & Zuo, X. (2023). Numerical investigation on the height and intensity variations of sporadic E layers at mid-latitude. *Journal of Geophysical Research: Space Physics*, *128*(9), e2023JA031508. https://doi.org/10.1029/2023ja031508

Qiu, L., Zuo, X., Yu, T., Sun, Y., & Qi, Y. (2019). Comparison of global morphologies of vertical ion convergence and sporadic E occurrence rate. *Advances in Space Research*, *63*(11), 3606–3611. https://doi.org/10.1016/j.asr.2019.02.024

Resende, L. C., Arras, C., Batista, I. S., Denardini, C. M., Bertollotto, T., & Moro, J. (2018). Study of sporadic E layers based on GPS radio occultation measurements and digisonde data over the Brazilian region. *Annales Geophysicae*, *36*(2), 587–593. https://doi.org/10.5194/angeo-36-587-2018

Resende, L. C. A., Batista, I. S., Denardini, C. M., Batista, P. P., Carrasco, A. J., de Fátima Andrioli, V., & Moro, J. (2017). Simulations of blanketing sporadic E-layer over the Brazilian sector driven by tidal winds. *Journal of Atmospheric and Solar-Terrestrial Physics*, *154*, 104–114. https://doi.org/10.1016/j.jastp.2016.12.012

Salby, M. L. (1981a). Rossby normal modes in nonuniform background configurations. Part I: Simple fields. *Journal of the Atmospheric Sciences*, *38*(9), 1803–1826. https://doi.org/10.1175/1520-0469(1981)038<1803:rnminb>2.0.co;2

Salby, M. L. (1981b). Rossby normal modes in nonuniform background configurations. Part II. Equinox and solstice conditions. *Journal of the Atmospheric Sciences*, *38*(9), 1827–1840. https://doi.org/10.1175/1520-0469(1981)038<1827:rnminb>2.0.co;2

Salby, M. L. (1984). Survey of planetary-scale traveling waves: The state of theory and observations. *Reviews of Geophysics*, *22*(2), 209–236. https://doi.org/10.1029/rg022i002p00209

Schreiner, W. S., Weiss, J., Anthes, R. A., Braun, J., Chu, V., Fong, J., et al. (2020). COSMIC-2 radio occultation constellation: First results. *Geophysical Research Letters*, *47*(4), e2019GL086841. https://doi.org/10.1029/2019gl086841

Schwartz, M. J., Lambert, A., Manney, G. L., Read, W. G., Livesey, N. J., Froidevaux, L., et al. (2008). Validation of the aura microwave limb sounder temperature and geopotential height measurements. *Journal of Geophysical Research*, *113*(D15), D15S11. https://doi.org/10.1029/2007jd008783

Shalimov, S., & Haldoupis, C. (2002). A model of mid-latitude E-region plasma convergence inside a planetary wave cyclonic vortex. *Annales Geophysicae*, *20*(8), 1193–1201. https://doi.org/10.5194/angeo-20-1193-2002

Shalimov, S., Haldoupis, C., Voiculescu, M., & Schlegel, K. (1999). Midlatitude E region plasma accumulation driven by planetary wave horizontal wind shears. *Journal of Geophysical Research*, *104*(A12), 28207–28213. https://doi.org/10.1029/1999ja900316

Shinagawa, H., Miyoshi, Y., Jin, H., & Fujiwara, H. (2017). Global distribution of neutral wind shear associated with sporadic E layers derived from GAIA. *Journal of Geophysical Research: Space Physics*, *122*(4), 4450–4465. https://doi.org/10.1002/2016ja023778

Sobhkhiz-Miandehi, S., Yamazaki, Y., Arras, C., Miyoshi, Y., & Shinagawa, H. (2022). Comparison of the tidal signatures in sporadic E and vertical ion convergence rate, using FORMOSAT-3/COSMIC radio occultation observations and GAIA model. *Earth Planets and Space*, *74*(1), 1–13. https://doi.org/10.1186/s40623-022-01637-y

Sobhkhiz-Miandehi, S., Yamazaki, Y., Arras, C., & Themens, D. (2023). A comparison of FORMOSAT-3/COSMIC radio occultation and ionosonde measurements in sporadic E detection over mid and low latitude regions. *Frontiers in Astronomy and Space Sciences*, *10*, 1198071. https://doi.org/10.3389/fspas.2023.1198071

Spire Repository. (2024). UCAR website [Dataset]. Retrieved from https://data.cosmic.ucar.edu/gnss-ro/spire/noaa/nrt/level1b/

Tarpley, J., & Matsushita, S. (1971). The lunar tide in ƒbEs. *Radio Science*, *6*(2), 191–196. https://doi.org/10.1029/rs006i002p00191

Tsunoda, R. T., Yamamoto, M., Igarashi, K., Hocke, K., & Fukao, S. (1998). Quasi-periodic radar echoes from midlatitude sporadic E and role of the 5-day planetary wave. *Geophysical Research Letters*, *25*(7), 951–954. https://doi.org/10.1029/98gl00663

Voiculescu, M., Haldoupis, C., Pancheva, D., Ignat, M., Schlegel, K., & Shalimov, S. (2000). More evidence for a planetary wave link with midlatitude E region coherent backscatter and sporadic E layers. *Annales Geophysicae*, *18*(9), 1182–1196. https://doi.org/10.1007/s005850000261

Voiculescu, M., Haldoupis, C., & Schlegel, K. (1999). Evidence for planetary wave effects on midlatitude backscatter and sporadic E layer occurrence. *Geophysical Research Letters*, *26*(8), 1105–1108. https://doi.org/10.1029/1999gl900172

Vondrak, T., Plane, J. M. C., Broadley, S., & Janches, D. (2008). A chemical model of meteoric ablation. *Atmospheric Chemistry and Physics*, *8*(23), 7015–7031. https://doi.org/10.5194/acp-8-7015-2008

Wakai, N., Ohyama, H., & Koizumi, T. (1987). *Manual of ionogram scaling*. Radio Research Laboratory, Ministry of Posts and Telecommunications.

Wang, J., Zuo, X., Sun, Y. Y., Yu, T., Wang, Y., Qiu, L., et al. (2021). Multilayered sporadic-E response to the annular solar eclipse on June 21, 2020. *Space Weather*, *19*(3), e2020SW002643. https://doi.org/10.1029/2020sw002643

Waters, J. W., Froidevaux, L., Harwood, R. S., Jarnot, R. F., Pickett, H. M., Read, W. G., et al. (2006). The Earth observing system microwave limb sounder (EOS MLS) on the Aura satellite. *IEEE Transactions on Geoscience and Remote Sensing*, *44*(5), 1075–1092. https://doi.org/10.1109/tgrs.2006.873771

Whitehead, J. (1961). The formation of the Sporadic-E layer in the temperate zones. *Journal of Atmospheric and Terrestrial Physics*, *20*(1), 49–58. https://doi.org/10.1016/0021-9169(61)90097-6

Whitehead, J. (1970). Production and prediction of sporadic E. *Reviews of Geophysics*, *8*(1), 65–144. https://doi.org/10.1029/rg008i001p00065

Whitehead, J. (1989). Recent work on mid-latitude and equatorial Sporadic-E. *Journal of Atmospheric and Terrestrial Physics*, *51*(5), 401–424. https://doi.org/10.1016/0021-9169(89)90122-0

Wu, D. L., Ao, C. O., Hajj, G. A., de La Torre Juarez, M., & Mannucci, A. J. (2005). Sporadic E morphology from GPS-CHAMP radio occultation. *Journal of Geophysical Research*, *110*(A1), A01306. https://doi.org/10.1029/2004ja010701

Yamazaki, Y. (2018). Quasi-6-day wave effects on the equatorial ionization anomaly over a solar cycle. *Journal of Geophysical Research: Space Physics*, *123*(11), 9881–9892. https://doi.org/10.1029/2018ja026014

Yamazaki, Y. (2023). A method to derive Fourier–wavelet spectra for the characterization of global-scale waves in the mesosphere and lower thermosphere and its MATLAB and Python software (fourierwavelet v1. 1). *Geoscientific Model Development*, *16*(16), 4749–4766. https://doi.org/10.5194/gmd-16-4749-2023

Yamazaki, Y. (2023b). MATLAB and Python software to compute Fourier-wavelet spectra (fourierwavelet v1.2) using longitude-time data for studying global-scale atmospheric waves [Software]. In *Geoscientific model development (v1.2)*. https://doi.org/10.5281/zenodo.10000479

Yamazaki, Y., Arras, C., Andoh, S., Miyoshi, Y., Shinagawa, H., Harding, B., et al. (2022). Examining the wind shear theory of sporadic E with ICON/MIGHTI winds and COSMIC-2 radio occultation data. *Geophysical Research Letters*, *49*(1), e2021GL096202. https://doi.org/10.1029/2021gl096202

Yamazaki, Y., & Matthias, V. (2019). Large-amplitude quasi-10-day waves in the middle atmosphere during final warmings. *Journal of Geophysical Research: Atmospheres*, *124*(17–18), 9874–9892. https://doi.org/10.1029/2019jd030634

Yamazaki, Y., Matthias, V., & Miyoshi, Y. (2021). Quasi-4-Day wave: Atmospheric manifestation of the first symmetric Rossby normal mode of zonal wavenumber 2. *Journal of Geophysical Research: Atmospheres*, *126*(13), e2021JD034855. https://doi.org/10.1029/2021jd034855

Yamazaki, Y., Miyoshi, Y., Xiong, C., Stolle, C., Soares, G., & Yoshikawa, A. (2020). Whole atmosphere model simulations of ultrafast Kelvin wave effects in the ionosphere and thermosphere. *Journal of Geophysical Research: Space Physics*, *125*(7), e2020JA027939. https://doi.org/10.1029/2020ja027939

Yeh, W. H., Liu, J. Y., Huang, C. Y., & Chen, S. P. (2014). Explanation of the Sporadic-E layer formation by comparing FORMOSAT-3/COSMIC data with meteor and wind shear information. *Journal of Geophysical Research: Atmospheres*, *119*(8), 4568–4579. https://doi.org/10.1002/2013jd020798

Yu, B., Xue, X., Scott, C. J., Yue, X., & Dou, X. (2022). An empirical model of the ionospheric sporadic E layer based on GNSS radio occultation data. *Space Weather*, *20*(8), e2022SW003113. https://doi.org/10.1029/2022sw003113

Yue, J., Lieberman, R., & Chang, L. C. (2021). Planetary waves and their impact on the mesosphere, thermosphere, and ionosphere. *Upper Atmosphere Dynamics and Energetics*, 183–216. https://doi.org/10.1002/9781119815631.ch10

Zuo, X., & Wan, W. (2008). Planetary wave oscillations in sporadic E layer occurrence at Wuhan. *Earth Planets and Space*, *60*(6), 647–652. https://doi.org/10.1186/bf03353128

Zuo, X., Wan, W., & Zhao, G. (2009). An attempt to infer information on planetary wave by analyzing sporadic E layers observations. *Earth Planets and Space*, *61*(10), 1185–1190. https://doi.org/10.1186/bf03352970